Probing Ligand Effects on the Redox Energies of [4Fe−4S] Clusters Using Broken-Symmetry Density Functional Theory

Shuqiang Niu and Toshiko Ichiye*

Department of Chemistry, Georgetown University, Washington, DC 20057-1227

Received: October 24, 2008; Revised Manuscript Received: February 23, 2009

A central issue in understanding redox properties of iron−sulfur proteins is determining the factors that tune the reduction potentials of the Fe−S clusters. Recently, Solomon and coworkers have shown that the Fe−S bond covalency of protein analogs measured by %L, the percent ligand character of the Fe 3d orbitals, from ligand K-edge X-ray absorption spectroscopy (XAS) correlates with the electrochemical redox potentials. Also, Wang and coworkers have measured electron detachment energies for iron−sulfur clusters without environmental perturbations by gas-phase photoelectron spectroscopy (PES). Here the correlations of the ligand character with redox energy and %L character are examined in $[Fe_4S_4L_4]^{2-}$ clusters with different ligands by broken symmetry density functional theory (BS-DFT) calculations using the B3LYP functional together with PES and XAS experimental results. These gas-phase studies assess ligand effects independently of environmental perturbations and thus provide essential information for computational studies of iron−sulfur proteins. The B3LYP oxidation energies agree well with PES data, and the %L character obtained from natural bond orbital analysis correlates with XAS values, although it systematically underestimates them because of basis set effects. The results show that stronger electron-donating terminal ligands increase $\%L_t$, the percent ligand character from terminal ligands, but decrease $\%S_b$, the percent ligand character from the bridging sulfurs. Because the oxidized orbital has significant Fe−L_t antibonding character, the oxidation energy correlates well with $\%L_t$. However, because the reduced orbital has varying contributions of both Fe−L_t and Fe−S_b antibonding character, the reduction energy does not correlate with either $\%L_t$ or $\%S_b$. Overall, BS-DFT calculations together with XAS and PES experiments can unravel the complex underlying factors in the redox energy and chemical bonding of the [4Fe−4S] clusters in iron−sulfur proteins.

Introduction

As one of the most ubiquitous and versatile electron carriers, [4Fe−4S] clusters play an important role in biological electron transfer as well as in biosynthetic and bioregulatory functions.[1,2] Determining the factors that tune the reduction potentials of these clusters in proteins is crucial for understanding their structure−function relationships.[3,4] However, probing the environmental effects is difficult because of the complexity of the protein environment. Advances in experimental methods and computational chemistry offer the opportunity for detailed investigations of the complex electronic structure and redox properties of the iron−sulfur clusters found in proteins. For instance, gas-phase photodetachment photoelectron spectroscopy (PES) is an experimental probe of the electronic structure and energetics of clusters, independent of environmental perturbations such as solvent, crystal field, or surrounding protein,[5] whereas X-ray absorption spectroscopy (XAS) provides a direct experimental probe of the ligand−metal bond covalency by determining the percent of ligand orbital mixing in the Fe 3d orbitals.[6] In addition, broken symmetry density functional theory (BS-DFT) calculations provide accurate results for the complex spin properties of the multi-iron Fe−S clusters.[7,8] Moreover, the density functionals and basis sets in our BS-DFT calculations have been calibrated by extensive comparisons of experimental and theoretical results for gas-phase Fe−S clusters by Wang and coworkers and our group.[9] Our BS-DFT calculations can now provide not only interpretations of experimental data[5,10] but also more extensive information about the electronic structure, chemical bonding, and energetics, especially for those states not easily accessible by experiments.[11]

BS-DFT calculations of $[Fe_4S_4(SCH_3)_4]^{2-}$ by Noodleman, Case, and coworkers[7] suggest that the antiferromagnetically spin-coupled $[4Fe-4S]^{2+}$ core ($S = 0$) consists of two high-spin ferromagnetic $[2Fe-2S]^{+}$ redox layers ($S = 9/2$). In each redox layer, the majority spins are located at the two irons ($S_i = 5/2$), and the minority spin ($s_i = 1/2$) is usually delocalized between the two irons (Figure 1a), resulting in two identical irons that can be described as having $Fe^{+2.5}$ character. The interaction between the high-spin iron sites with strong spin polarization and the bridging sulfides and the terminal ligands generally leads to an unusual energy level pattern (the "inverted level scheme") in which the metal−ligand lone pair orbitals lie between the split metal orbitals (Figure 1b), thus giving rise to a shift in electron density from the terminal ligands to the $[4Fe-4S]^{2+}$ core. The minority spin in the highest occupied molecular orbital (HOMO) of a given redox layer of $[Fe_4S_4L_4]^{2-}$ is delocalized in the σ_{Fe-Fe} orbitals, which also have apparent σ^*_{Fe-L} antibonding character, whereas the lowest unoccupied molecular orbitals (LUMOs) have σ^*_{Fe-Fe} and σ^*_{Fe-S} but less σ^*_{Fe-L} antibonding character (Figure 1).[5]

Recently, sulfur K-edge XAS studies on a series of Fe−S protein analogs by Solomon and coworkers indicate that the covalencies of the Fe−S bonds of the clusters correlate with their electrochemical redox potentials.[12−15] The bond covalencies were described by %L, the percent ligand character of the Fe

* To whom correspondence should be addressed. E-mail: ti9@georgetown.edu.

10.1021/jp809446q CCC: $40.75
Published on Web 04/20/2009

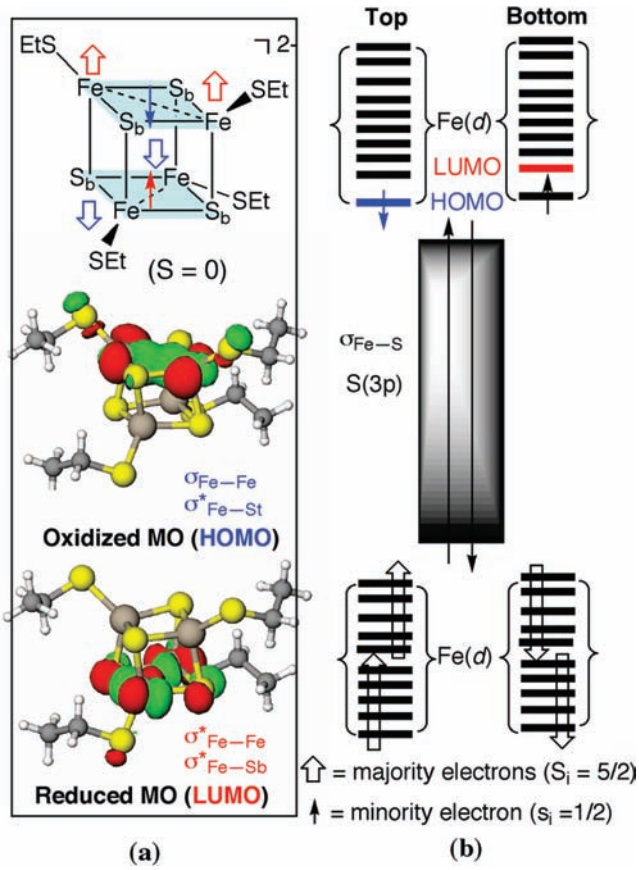

Figure 1. Schematic (a) structure, HOMO, and LUMO and (b) molecular orbitals of $[Fe_4S_4(SEt)_4]^{2-}$ (SEt = SC_2H_5). The long arrows represent the electrons of the ligand lone pairs and σ_{Fe-S} bonds, the small arrows represent the minority spin electrons (s_i = 1/2), and the large hollow arrows represent the d^5 majority-spin electrons (S_i =5/2).

3d orbitals as determined from the intensity of the pre-edge features of the ligand K-edge. Interestingly, significant differences in the experimental %L character were found between the high-potential iron−sulfur proteins (HiPIPs) and ferredoxins (Fds)[12,13] and between $[Fe_4S_4(SBut)_4]^{2-}$ and hydrogen-bonded $[Fe_4S_4(SBut)_4]^{2-}$ (SBut = *S*-*t*-butyl).[16] However, the covalency of the Fe−S bond reflects the electronic structure of the initial state $[Fe_4S_4(SR)_4]^{2-}$ cluster and thus directly affects the vertical oxidation or reduction energies to the $[Fe_4S_4(SR)_4]^{1-}$ or $[Fe_4S_4(SR)_4]^{3-}$ state, respectively, whereas electrochemical redox potentials have a variety of factors that affect their values, making their interpretation difficult. For instance, significant electronic and structural relaxation[5,7,8,17] are important in the electrochemical redox potentials, so the adiabatic detachment and reduction energies (ADE and ARE, respectively) reflect the electronic and structural properties of the $[Fe_4S_4(SR)_4]^{1-}$ and $[Fe_4S_4(SR)_4]^{3-}$ states, respectively, as well as those of $[Fe_4S_4(SR)_4]^{2-}$ probed in the XAS experiments. In addition, the electrochemical redox potentials contain a large contribution due to the environment of the cluster, whether solvent or a protein matrix plus solvent, which is not expected to be correlated to the covalency of the Fe−S bonds. Therefore, the %L character should be more directly correlated to the vertical detachment and reduction energies (VDE and VRE, respectively) of clusters in the gas phase rather than the electrochemical redox potentials.

Here, in conjunction with ligand K-edge XAS and PES experimental results, the electronic effects of different ligands on the covalency of the Fe−L bonds and on redox energies of the [4Fe−4S] clusters in the gas phase are explored by BS-DFT calculations. Because the PES experiments can measure only the VDE of $[Fe_4S_4L_4]^{2-}$, the BS-DFT calculations are shown to reproduce the VDE from PES and are then used to calculate VRE. These calculations are also shown to give %L character that correlates well with values from PES. This allows an internally consistent comparison of the correlation of the gas phase %L character with the gas phase VDE and VRE without complications due to geometric and electronic relaxation or solvent effects. Calculations were performed for $[Fe_4S_4L_4]^{2-}$ with a variety of terminal ligands, L, where L = H, Cl, Br, I, Ac, SH, SMe, SeMe, SEt, SBut, PH_2, or PMe_2 (Ac = acetate, Me = methyl, Et = ethyl, But = *t*-butyl) so that the effects of the electron-donating ability of the ligands could be examined.

Methods

Because the systems here involve antiferromagnetically spin-coupled interactions, the broken symmetry (BS) approach[7,8] for the DFT calculations[18] was employed to account for antiferromagnetic spin interactions in the exchange−correlation energy functionals. Becke's three-parameter hybrid exchange[19] and Lee−Yang−Parr correlation functional (B3LYP)[20] using the 6-31G** basis sets[21−23] were utilized for the geometry optimizations and electronic structure calculations of the [4Fe−4S] clusters. No symmetry restraints were imposed during geometry optimizations. The calculated energies were refined at the B3LYP/6-31(++)$_S$G**//B3LYP/6-31G** level, where (++)$_S$ indicates that sp-type diffuse functions were added to the 6-31G** basis set for the sulfur atoms.[21−23] No approximate spin projection procedures[7,8,24] were used to optimize the geometries or to correct the energies for the BS-DFT approach (see infra). We obtained the VDE and VRE of $[Fe_4S_4L_4]^{2-}$ by calculating the energy difference between $[Fe_4S_4L_4]^{2-}$ and $[Fe_4S_4L_4]^{-}$ and between $[Fe_4S_4L_4]^{2-}$ and $[Fe_4S_4L_4]^{3-}$, respectively, using the $[Fe_4S_4L_4]^{2-}$ geometry.

The σ-electron donating ability of the terminal ligands, L, was evaluated by the proton affinity (PA), defined as the difference in the calculated energies of the optimized L−H and L^- in the gas phase. Although the calculations did not take enthalpy effects into account, the calculated PAs at the B3LYP/6-31G** level are in good agreement with molecular acidity measured by experiments in the gas phase.[25]

Natural bond orbital (NBO) analyses[26] were performed to obtain charges and %L character. The $[Fe_4S_4L_4]^{2-}$ cluster consists of 4 iron-terminal ligand (Fe−L_t) bonds and 12 iron-bridging ligand (Fe−S_b) bonds (top of Figure 1a). In the "inverted level scheme", the doubly occupied Fe−L and ligand lone pair orbitals lie between the split 20 Fe majority spin and 2 minority spin orbitals (Figure 1b). The high-lying 9 α and 9 β unoccupied orbitals of the singly occupied Fe 3d orbitals form transition-accepting holes from the ligand 1s orbitals. Because the 18 Fe 3d orbital holes can be represented by the unoccupied orbitals of the 16 singly occupied Fe−L bond orbitals, the %L character from the bridging sulfurs and the terminal ligands can be directly obtained from these unoccupied orbitals. Similar to the experimental work,[12,15] the total %L character is defined here as the sum of $\%S_{3p}(b)$ and $\%L_{np}(t)$, where $\%S_{3p}(b)$ is the percent bridging sulfur 3p character summed over each of the 12 Fe−S_b bonds, and $\%L_{np}(t)$ is the percent terminal ligand np character summed over each of the 4 Fe−L_t bonds.

All calculations were performed using the NWChem program package.[27] The molecular orbital visualizations were performed using the extensible computational chemistry environment (Ecce) application software.[28]

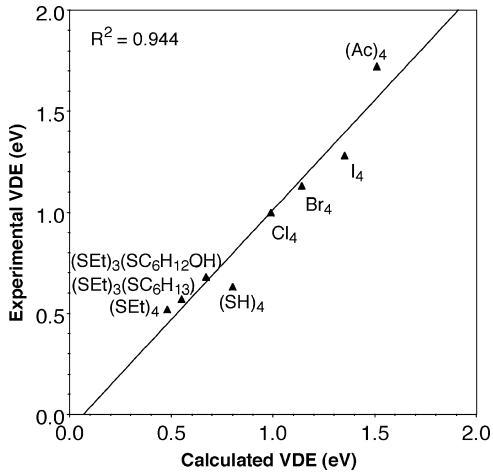

Figure 2. Correlation of the calculated VDEs with experimental VDEs of $[Fe_4S_4L_4]^{2-}$ (Et = ethyl, Ac = acetate); $R^2 = 0.944$.

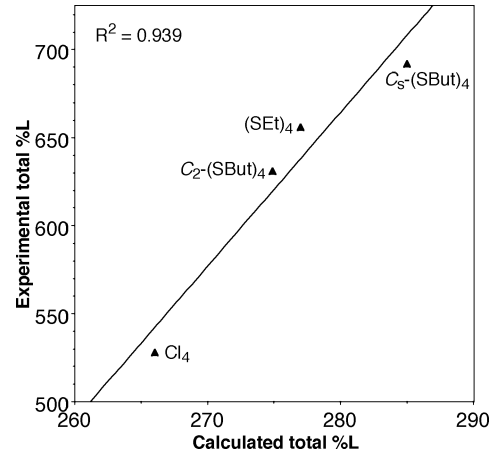

Figure 3. Correlation of the calculated total %L with experimental %L of $[Fe_4S_4(SR)_4]^{2-}$ (But = *t*-butyl); $R^2 = 0.939$. (See the Methods section for definitions.)

Results and Discussion

Density Functional Theory Calculations of Redox Energies and Fe−L Covalency. Our BS-DFT calculations at the B3LYP/6-31(++)$_S$G**//B3LYP/6-31G** level of metallic clusters can reproduce a wide variety of experimental results including redox energies.[5,11,29] Here the calculated VDE and ADE for [4Fe−4S] clusters with a wide variety of ligands in the gas phase are in excellent agreement with results from gas-phase PES measurements of the same clusters (Figure 2 and Figure S1 in the Supporting Information). In particular, our studies of $[Fe(SCH_3)_4]^{n-}$ and $[Fe(SCH_3)_3]^{n-}$ clusters in different oxidation states show that adding diffuse function to the sulfur basis in double-ζ basis sets for the energy calculations gives excellent results in comparison with experiment,[9] and our studies of $[FeX_4]^{1-}$ (X = Cl, Br) and $[FeX_3]^{1-}$ (M = Mn, Fe, Co, Ni, X = Cl, Br) show that increasing the basis set size for all atoms to the triple-ζ basis set does not significantly improve agreement with experiment.[30] In addition, although the BS state energy is not a pure spin state energy because the BS approach utilizes a single determinant for a spin-coupled low-spin state, the potential energy surface of a ground state with large spin-coupled numbers appears to be close to that of the true ground state because a BS state is a weighted average of pure-spin states.[7,8,24] Furthermore, the error arising from spin contamination of higher-spin states tends to cancel in calculations of redox or other relative energies.[5] Therefore, approximate spin projection procedures[7,8,24] were not used to correct the energies.

In addition, the calculated total %L character of the metal−ligand bonds of [4Fe−4S] clusters with different ligands in the gas phase correlates well with ligand K-edge XAS measurements of the same clusters in the solid phase (Figure 3).[6,16,31] However, the magnitude of the NBO values for the total %L character are about 50−58% less than the experimental values. Although the B3LYP/6-31(++)$_S$G**//B3LYP/6-31G** energies have been thoroughly tested and compared against PES data,[9] the calibration of the %L is just underway. The B3LYP/6-31G** and B3LYP/6-31(++)$_S$G** basis sets give essentially the same %L character, and the slight overestimation of the Fe−S bond lengths by B3LYP/6-31G** with respect to X-ray data[5,11,29] has been ruled out as a cause because the total %L character calculated for the experimental $[Fe_4S_4(SEt)_4]^{2-}$ structure is only ∼2% smaller than that for the B3LYP geometry. However, comparisons with NBO analysis using the DFT optimized double-ζ split valence basis sets with polarization function (DZVP)[32] on the B3LYP/6-31G** geometry indicate that the σ contribution is underestimated, although the VTZ triple-ζ basis sets[33] actually give values closer to those from the B3LYP/6-31G** basis sets. Moreover, the optimization of $[Fe_4S_4(SMe)_4]^{2-}$ at the B3LYP/VTZ level gives unusual structures. Given these inconsistencies, further studies are underway to compare the use of DZVP and 6-31G** basis sets for consistent calculations of geometry, redox energies, and covalencies. However, the good correlation between the %L from B3LYP/6-31G** with experiment indicates that the errors are likely to be systematic errors due to the NBO analysis, which is basis-set dependent, as is any orbital-based approach.[34] Because at this point the energies have been calibrated for only B3LYP/6-31(++)$_S$G**//B3LYP/6-31G**, the current NBO analysis using the 6-31G** seems warranted for investigation of the underlying effects of different ligands on the redox energetics and bonding of these clusters.

Ligand Effects on the Fe−L Covalency. The nature of the ligands in an analog consisting of a $[4Fe-4S]^{2+}$ core bound by four terminal ligands is expected to affect its electronic properties. A range of ligands were investigated, including a cluster with strong electron donor ligands, $[Fe_4S_4H_4]^{2-}$, although the Fe−H $\%L_{1s}(t)$ is not accessible by XAS experiments. The ligands can be primarily characterized by their σ-electron donating ability, which can be assessed by the calculated PA of the ligand alone; that is, ligands with greater PA should be more able to donate σ electrons. The calculated net charge of the $[4Fe-4S]^{2+}$ core bound by a given set of terminal ligands, which is a measure of how much electron donation has occurred from the ligands to the core, correlates well with the calculated PA of the terminal ligands (Figure 4). Because the net charge decreases with greater electron-donating ability, the PA calculated for the terminal ligand alone is a good predictor of the degree of electron donation from the ligands to the core when the terminal ligand is bound in the cluster.

The net charge of the $[4Fe-4S]^{2+}$ core is also an indicator of the covalency of the Fe−L_t bonds of $[Fe_4S_4L_4]^{2-}$ because the greater donation of electrons by the terminal ligands to the core (i.e., lower net charge) implies stronger ligand−metal bonding interactions and thus a more covalent bond. The calculated $\%L_{np}(t)$ character of the Fe 3d orbitals (Methods section) increases with decreasing $[4Fe-4S]^{2+}$ charge (Figure 5), which indicates that the Fe−L_t bonds become stronger as the electron density is shifted from the ligands to the core.

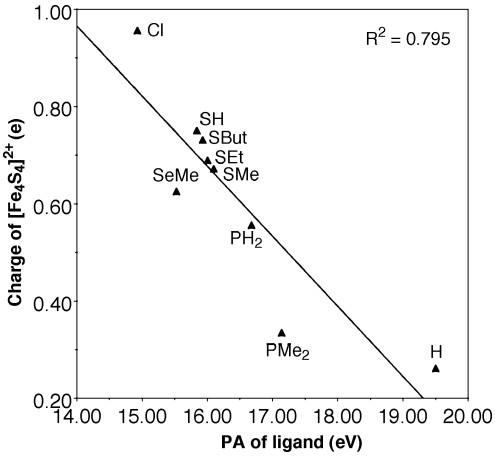

Figure 4. Correlation of calculated proton affinity (PA) of the ligand (L) with the NBO charge of the $[4Fe-4S]^{2+}$ core of $[Fe_4S_4L_4]^{2-}$; $R^2 = 0.795$.

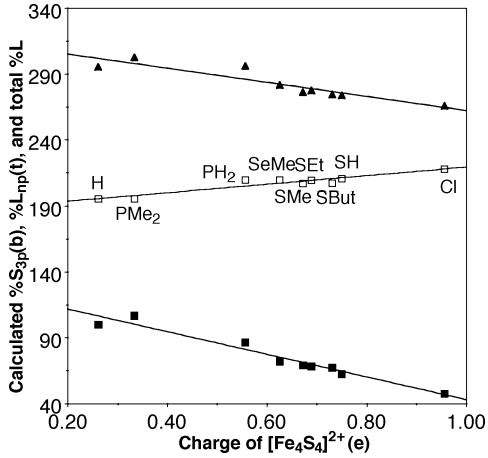

Figure 5. Correlation of the NBO charge of the $[4Fe-4S]^{2+}$ core with the calculated total %L (▲, $R^2 = 0.843$), bridging $\%S_{3p}$(b) (□, $R^2 = 0.887$), and terminal $\%L_{np}$(t) (■, $R^2 = 0.951$) of $[Fe_4S_4L_4]^{2-}$.

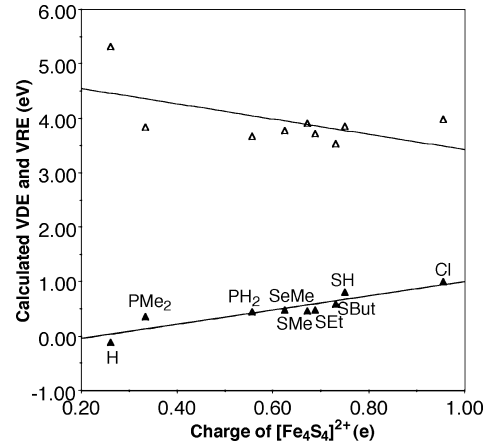

Figure 6. Correlation of the NBO charge of the $[4Fe-4S]^{2+}$ core with the calculated VDE (▲, $R^2 = 0.833$) and VRE (△, $R^2 = 0.320$) of $[Fe_4S_4L_4]^{2-}$.

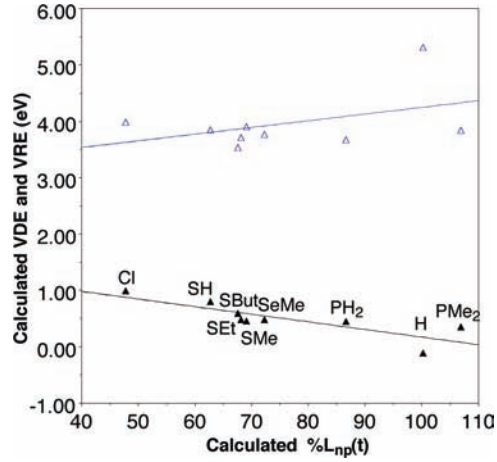

Figure 7. Correlation of the calculated terminal $\%L_{np}$(t) with calculated VDE (▲, $R^2 = 0.686$) and VRE (△, $R^2 = 0.178$).

However, the calculated $\%S_{3p}$(b) character (Methods section) decreases with decreasing $[4Fe-4S]^{2+}$ charge (Figure 5), which indicates that as more electron density shifts from the terminal ligands to the core, electron density is also shifted from the irons to the bridging sulfurs, thus weakening the $Fe-S_b$ bonds. However, the $\%L_{np}$(t) character depends more strongly on the $[4Fe-4S]^{2+}$ charge than the $\%S_{3p}$(b) character does, so the total %L character increases with decreasing $[4Fe-4S]^{2+}$ charge. Therefore, the terminal ligand electronic effects are directly reflected in $\%L_{np}$(t) character but also dominate the total %L character.

Fe−L Covalency Effects on the Redox Energy. Because the oxidation and reduction of $[Fe_4S_4L_4]^{2-}$ clusters involve orbitals that have varying degrees of σ^*_{Fe-S} and σ^*_{Fe-L} antibonding characters, the redox properties are expected to depend on the electronic properties of the ligands. Because of the large σ^*_{Fe-L} antibonding character of the oxidized HOMO, the calculated VDE of $[Fe_4S_4L_4]^{2-}$ decreases with decreasing calculated NBO charge of the $[4Fe-4S]^{2+}$ core (Figure 6) and increasing calculated $\%L_{np}$(t) character (Figure 7). This implies that the oxidation energy decreases with the degree of electron donation from the terminal ligands and the covalency of the $Fe-L_t$ bonds. However, the calculated VRE of $[Fe_4S_4L_4]^{2-}$ is essentially uncorrelated with the net charge of the $[4Fe-4S]^{2+}$ core (Figure 6) and the $\%L_{np}$(t) character (Figure 7) or the $\%S_{3p}$(b) or total %L character (Figures S2 and S3 in the Supporting Information), presumably because of the smaller σ^*_{Fe-L} and larger σ^*_{Fe-S} character of the reduced LUMO. Apparently, the energy of the LUMO has a complicated dependence on the terminal ligands because of the secondary effect of decreasing donation from the bridging ligands with increasing donation from the terminal ligands. Therefore, the reduction energy does not simply correlate with the degree of electron donation from the terminal ligands to the core. Note that the analog with the hydride ligands, $[Fe_4S_4H_4]^{2-}$, shows significant differences from the other ligands, but because its VDE is actually slightly negative, indicating that the cluster is more stable in the $[4Fe-4S]^{3+}$ state, it is not surprising that the energetics do not follow the trends of the other clusters (Figure 6 and 7).

Conclusions

BS-DFT calculations, in conjunction with PES and ligand K-edge XAS techniques, are powerful probes of the electronic structure, chemical bonding, and redox properties of [4Fe−4S] clusters. Here B3LYP calculations of the redox energy and the ligand character of Fe 3d orbitals in a series of [4Fe−4S] clusters with different ligands have been performed. The calculated oxidation energies are in very good agreement with the PES measured values in the gas phase, and the calculated total %L correlates well with the ligand K-edge XAS measurements in the solid, although the current NBO analysis at the B3LYP/6-

31G** level underestimates the magnitudes, mainly because of poorer flexibility and good electron correlation in the Hartree−Fock-optimized basis sets.[32]

Our calculations show that the properties of the terminal ligands influence the covalency of all of the Fe−L bonds. The NBO charge of the [4Fe−4S] core, which is a measure of the electron donation from the ligands and thus of the covalency of the Fe−L_t bonds, correlates with the electron-donating ability of the terminal ligands of clusters. The $\%L_{np}(t)$ character mixing in the Fe 3d orbitals increases with decreasing NBO charge of the [4Fe−4S] core and is also a measure of the covalency of the Fe−L_t bonds. However, the $\%S_{3p}(b)$ character decreases with decreasing NBO charge of the [4Fe−4S] core, indicating that increased donation from the terminal ligands is accompanied by decreased donation from the bridging sulfurs.

Finally, our calculations show that the redox energies have a complicated dependency on the covalency of the Fe−L bonds. The oxidation energy correlates well with the Fe−L_t covalency, as measured by either the NBO charge of the [4Fe−4S] core or the $\%L_{np}(t)$ character. The correlation arises because the oxidized minority spin electron is in a σ_{Fe-Fe} orbital with significant σ^*_{Fe-L} antibonding character. Therefore, good electron-donating ligands result in stronger Fe−L_t bonding interactions and lower oxidation energies of clusters. However, because the reduced electron involves a σ^*_{Fe-Fe} antibonding orbital with bridging σ^*_{Fe-S} as well as less σ^*_{Fe-L} antibonding character, the reduction energy has a complicated dependence on both the $\%S_{3p}(b)$ and $\%L_{np}(t)$ character. In particular, because the $\%L_{np}(t)$ tends to decrease as the $\%S_{3p}(b)$ increases, the influence of the ligands depends on whether the σ^*_{Fe-L} or σ^*_{Fe-S} contributes more to the σ^*_{Fe-Fe} antibonding orbital.

In summary, a central issue in probing and predicting redox properties of iron−sulfur proteins is to determine the factors responsible for tuning the reduction potentials in the active sites. B3LYP calculations can quantitatively elucidate the contribution of ligand electronic effects to the ligand−metal bonding and redox energies. Ultimately, the real interest is in understanding the correlation observed by Solomon and coworkers between the Fe−S bond covalency and the electrochemical redox potentials. However, a variety of factors such as electronic and structural relaxation as well as the environment may affect the redox potential in different ways than they affect the %L character of the bond. Our calculations showing the correlation between the gas-phase covalency and the gas-phase VDE/VRE are strong theoretical support for Solomon's observed correlation between experimental %L and electrochemical redox potential because they demonstrate that the covalency, whether measured by %L or by the net charge donated to the cluster by the terminal ligands, directly influences the energy required to remove or add an electron irrespective of the environment. Overall, the BS-DFT calculations in conjunction with ligand K-edge XAS and PES data can be an effective tool for understanding changes in the chemical bonding and redox properties of iron−sulfur proteins and analogues arising from environmental factors.

Acknowledgment. We thank Prof. Edward L. Solomon for the detailed experimental data of $[Fe_4S_4(SBut)_4]^{2-}$. This work was supported by a grant from the National Institutes of Health (GM-45303). The calculations were performed at the EMSL, a national user facility sponsored by the U.S. DOE's Office of Biological and Environmental Research and located at Pacific Northwest National Laboratory, operated for DOE by Battelle, under the grant GC3565 and GC20901. Additional computational resources were provided by the William G. McGowan Foundation.

Supporting Information Available: Correlation of the calculated ADEs with experimental ADEs of $[Fe_4S_4L_4]^{2-}$, $R^2 = 0.977$, and the correlation of the $\%S_{3p}(b)$ and total %L with the calculated VDE and VRE. This material is available free of charge via the Internet at http://pubs.acs.org.

References and Notes

(1) Beinert, H.; Holm, R. H.; Münck, E. *Science* **1997**, *277*, 263.
(2) Beinert, H. *J. Biol. Inorg. Chem.* **2000**, *5*, 2.
(3) Ichiye, T. Computational Studies of Redox Potentials of Electron Transfer Proteins. In *Simulation and Theory of Electrostatic Interactions in Solution: Computational Chemistry, Biophysics, and Aqueous Solutions*, Proceedings of the AIP, Santa Fe, New Mexico, June 1999; Pratt, L. R., Hummer, G., Eds.; AIP: Melville, NY, 1999; Vol. 492, p 431.
(4) Ichiye, T. Simulations of Electron Transfer Proteins. In *Computational Biochemistry and Biophysics*; Becker, O. M., MacKerell, A. D., Jr., Roux, B., Watanabe, M., Eds.; Marcel Dekker: New York, 2001; p 393.
(5) Wang, X.-B.; Niu, S.-Q.; Yang, X.; Ibrahim, S. K.; Pickett, C. J.; Ichiye, T.; Wang, L.-S. *J. Am. Chem. Soc.* **2003**, *125*, 14072.
(6) Solomon, E. I.; Hedman, B.; Hodgson, K. O.; Dey, A.; Szilagyi, R. K. *Coord. Chem. Rev.* **2005**, *249*, 97.
(7) Noodleman, L.; Case, D. A. Density-Functional Theory of Spin Polarization and Spin Coupling in Iron−Sulfur Clusters. In *Advances in Inorganic Chemistry*; Cammack, R., Ed.; Academic Press: San Diego, 1992; Vol. 38, p 423.
(8) Noodleman, L.; Peng, C. Y.; Case, D. A.; Mouesca, J. M. *Coord. Chem. Rev.* **1995**, *144*, 199.
(9) Niu, S.-Q.; Nichols, J. A.; Ichiye, T. *J. Chem. Theory Comput.* **2009**, in press.
(10) Yang, X.; Niu, S.; Ichiye, T.; Wang, L.-S. *J. Am. Chem. Soc.* **2004**, *126*, 15790.
(11) Niu, S.-Q.; Wang, X.-B.; Yang, X.; Wang, L.-S.; Ichiye, T. *J. Phys. Chem. A* **2004**, *108*, 6750.
(12) Dey, A.; Francis, E. J.; Adams, M. W. W.; Babini, E.; Takahashi, Y.; Fukuyama, K.; Hodgson, K. O.; Hedman, B.; Solomon, E. I. *Science* **2007**, *318*, 1464.
(13) Glaser, T.; Bertini, I.; Moura, J. J. G.; Hedman, B.; Hodgson, K. O.; Solomon, E. I. *J. Am. Chem. Soc.* **2001**, *123*, 4859.
(14) Glaser, T.; Rose, K.; Shadle, S. E.; Hedman, B.; Hodgson, K. O.; Solomon, E. I. *J. Am. Chem. Soc.* **2001**, *123*, 442.
(15) Dey, A.; Glaser, T.; Couture, M. M. J.; Eltis, L. D.; Holm, R. H.; Hedman, B.; Hodgson, K. O.; Solomon, E. I. *J. Am. Chem. Soc.* **2004**, *126*, 8320.
(16) Dey, A.; Roche, C. L.; Walters, M. A.; Hodgson, K. O.; Hedman, B.; Solomon, E. I. *Inorg. Chem.* **2005**, *44*, 8349.
(17) Solomon, E. I.; Basumallick, L.; Chen, P.; Kennepohl, P. *Coord. Chem. Rev.* **2005**, *249*, 229.
(18) Parr, R. G.; Yang, W. *Density-Functional Theory of Atoms and Molecules*; Oxford University Press: Oxford, U.K., 1989.
(19) Becke, A. D. *J. Chem. Phys.* **1993**, *98*, 1372.
(20) Lee, C.; Yang, W.; Parr, R. G. *Phys. Rev.* **1988**, *B37*, 785.
(21) Rassolov, V.; Pople, J. A.; Ratner, M.; Windus, T. L. *J. Chem. Phys.* **1998**, *109*, 1223.
(22) Francl, M. M.; Petro, W. J.; Hehre, W. J.; Binkley, J. S.; Gordon, M. S.; DeFrees, D. J.; Pople, J. A. *J. Chem. Phys.* **1982**, *77*, 3654.
(23) Hariharan, P. C.; Pople, J. A. *Theor. Chim. Acta* **1973**, *28*, 213.
(24) Mouesca, J. M.; Chen, J. L.; Noodleman, L.; Bashford, D.; Case, D. A. *J. Am. Chem. Soc.* **1994**, *116*, 11898.
(25) Berkowitz, J.; Ellison, G. B.; Gutman, D. *J. Phys. Chem.* **1994**, *98*, 2744.
(26) Reed, A. E.; Curtiss, L. A.; Weinhold, F. *Chem. Rev.* **1988**, *88*, 899.
(27) Straatsma, T. P.; Aprà, E.; Windus, T. L.; Bylaska, E. J.; de Jong, W.; Hirata, S.; Valiev, M.; Hackler, M.; Pollack, L.; Harrison, R.; Dupuis, M.; Smith, D. M. A.; Nieplocha, J.; V., T.; Krishnan, M.; Auer, A. A.; Brown, E.; Cisneros, G.; Fann, G.; Früchtl, H.; Garza, J.; Hirao, K.; Kendall, R.; Nichols, J.; Tsemekhman, K.; Wolinski, K.; Anchell, J.; Bernholdt, D.; Borowski, P.; Clark, T.; Clerc, D.; Dachsel, H.; Deegan, M.; Dyall, K.; Elwood, D.; Glendening, E.; Gutowski, M.; Hess, A.; Jaffe, J.; Johnson, B.; Ju, J.; Kobayashi, R.; Kutteh, R.; Lin, Z.; Littlefield, R.; Long, X.; Meng, B.; Nakajima, T.; Niu, S.; Rosing, M.; Sandrone, G.; Stave, M.; Taylor, H.; Thomas, G.; van Lenthe, J.; Wong, A.; Zhang, Z., *NWChem: A Computational Chemistry Package for Parallel Computers*, version 4.6; Pacific Northwest National Laboratory: Richland, Washington, 2004.

(28) Black, G.; Didier, B.; Elsethagen, T.; Feller, D.; Gracio, D.; Hackler, M.; Havre, S.; Jones, D.; Jurrus, E.; Keller, T.; Lansing, C.; Matsumoto, S.; Palmer, B.; Peterson, M.; Schuchardt, K.; Stephan, E.; Taylor, H. T., G.; Vorpagel, E.; Windus, T.; Winters, C. *Ecce: A Problem Solving Environment for Computational Chemistry*, software version 3.2.1; Pacific Northwest National Laboratory: Richland, Washington, 2004.

(29) Niu, S.-Q.; Wang, X.-B.; Nichols, J. A.; Wang, L.-S.; Ichiye, T. *J. Phys. Chem. A* **2003**, *107*, 2898.

(30) Yang, X.; Wang, X.-B.; Wang, L.-S.; Niu, S.; Ichiye, T. *J. Chem. Phys.* **2003**, *119*, 8311.

(31) The experimental %S3p values of $[Fe_4S_4(S\text{-}t\text{-butyl})_4]^{2-}$ are from private communication with Prof. Solomon and experimental intensity of ref 15.

(32) Godbout, N.; Salahub, D. R.; Andzelm, J.; Wimmer, E. *Can. J. Chem.* **1992**, *70*, 560.

(33) Schafer, A.; Horn, H.; Ahlrichs, R. *J. Chem. Phys.* **1992**, *97*, 2571.

(34) Cramer, C. J. *Essentials of Computational Chemistry: Theories and Models*, 2nd ed.; Wiley: Chichester, U.K., 2004.

JP809446Q